Computers & Geosciences 88 (2016) 142–151

Contents lists available at ScienceDirect

Computers & Geosciences

journal homepage: www.elsevier.com/locate/cageo

Case study

Growth by Optimization of Work (GROW): A new modeling tool that predicts fault growth through work minimization

Jessica A. McBeck*, Elizabeth H. Madden, Michele L. Cooke

Department of Geosciences, University of Massachusetts Amherst, United States

ARTICLE INFO

Article history:
Received 15 May 2015
Received in revised form
28 December 2015
Accepted 29 December 2015
Available online 8 January 2016

Keywords:
Fault propagation
Work minimization
Hard-linkage
Soft-linkage
Boundary element method (BEM)
Numerical modeling
Propagation power
Releasing step

ABSTRACT

Growth by Optimization of Work (GROW) is a new modeling tool that automates fracture initiation, propagation, interaction, and linkage. GROW predicts fracture growth by finding the propagation path and fracture geometry that optimizes the global external work of the system. This implementation of work optimization is able to simulate more complex paths of fracture growth than energy release rate methods. In addition, whereas a Coulomb stress analysis determines two conjugate planes of potential failure, GROW identifies a single failure surface for each increment of growth. GROW also eliminates ambiguity in determining whether shear or tensile failure will occur at a fracture tip by assessing both modes of failure by the same propagation criterion. Here we describe the underlying algorithm of the program and present GROW models of two propagating faults separated by a releasing step. The discretization error of these models demonstrates that GROW can predict fault propagation paths within the numerical uncertainty produced by discretization. Model element size moderately influences the propagation paths, however, the final fault geometry remains similar between models with significantly different element sizes. The propagation power of the fault system, calculated from the change in work due to fault propagation, indicates when model faults interact through both soft- and hard-linkage.

1. Introduction

Understanding how faults evolve and interact at different stages of growth is fundamental to mitigating hazard in seismogenic regions. In addition, modeling fracture propagation, including joints and faults, provides insight into subsurface processes controlling the migration of water, ore-hosting fluids, and hydrocarbons. The new modeling tool Growth by Optimization of Work (GROW) uses a global work criterion to predict fracture propagation paths and interaction.

GROW provides an alternative to previous approaches of predicting fracture growth, which include the Hoek–Brown strength criteria (Hoek and Brown, 1980; 1997), the Drucker–Prager criterion (Drucker and Prager, 1952), and the Mogi criterion (Mogi, 1971). Another approach considers the energy release rate, or energy per unit area required to create new fracture surface, *G*. *G* is determined from the stress concentrations at a fracture tip (e.g., Irwin, 1958), which are controlled by the loading on, length and shape of the fracture (e.g., Griffith, 1924; McClintock and Walsh, 1962; Lajtai, 1971). The direction of growth that maximizes *G* predicts the collinear propagation path of opening-mode fractures subject to mode-I loading, such as joints, veins and dikes (e.g., Pollard and Aydin, 1988; and references therein) and the curved paths of opening-mode fractures under mixed-mode loading (e.g., Olson and Pollard, 1991; Cooke and Pollard, 1997; De Bremaecker and Ferris, 2004). *G* also provides a criterion for in-plane growth in shear (modes II or III) (e.g., Irwin, 1958). Although this criterion is applicable to certain materials, it struggles to predict the growth of faults within rock, where failure likely involves multiple, small-scale processes of tensile failure and linkage (e.g., Schultz, 1999; Crider and Peacock, 2004; Savalli and Engelder, 2005), which often result in complex propagation paths.

Previous analyses have predicted the propagation path of faults from the orientation of planes that maximize Coulomb stress (e.g., Crider and Pollard, 1998; Maerten et al., 2002; Olson and Cooke, 2005 ; Pollard and Fletcher, 2005). This approach determines two potential failure planes on which the ratio of shear to normal stress equals the internal coefficient of friction (Jaeger et al., 2007). If the material has anisotropic strength, one of the failure planes could be preferred; however, a robust numerical algorithm that determines which of the two planes fails is not generalizable for isotropic materials (Cooke and Madden, 2014). Furthermore, using a tensile failure criterion and maximum Coulomb stress in parallel can indicate that both tensile and shear failure are possible near a fracture tip, but this approach cannot unambiguously indicate

Abbreviations: GROW, GRowth by Optimization of Work; W_{ext}, external work; $W_{ext}/\Delta A$, external work divided by new fracture area

* Corresponding author.
E-mail address: jmcbeck@cns.umass.edu (J.A. McBeck).

http://dx.doi.org/10.1016/j.cageo.2015.12.019
0098-3004/

which failure mode is preferred (Cooke and Madden, 2014). Consequently, mode-specific failure criteria struggle to simulate how multiple faults may link and form one continuous structure. This linkage is a primary mechanism by which fault networks evolve (e.g., Crider and Peacock, 2004; and references therein).

GROW uses work minimization as an alternative method of predicting failure orientation and fracture propagation in intact rock. Numerous geologic problems related to the development of crustal faults have been investigated with work minimization, including slip-partitioning in transpressional environments (Jones and Wesnousky, 1992), fault geometry in southern California (Cooke and Kameda, 2002; Olson and Cooke, 2005), and the onset of kink-folding in heterogeneous material (Maillot and Leroy, 2006). Work minimization also has been used extensively to investigate the dynamics of accretionary systems, including the length of new accretionary forethrusts (Gutscher et al., 1998), the temporal evolution of thrusts within accretionary wedges (e.g., Hardy et al., 1998; Del Castello and Cooke, 2007; Cubas et al., 2008), and the distribution of stress in accretionary systems (e.g., Souloumiac et al., 2009, 2010; Yagupsky et al., 2014).

Cooke and Madden (2014) develop a general implementation of work minimization to predict fault and joint propagation paths with various failure modes and along complex propagation paths by assuming that the crust deforms to optimize the external work, W_{ext}, acting on the system. W_{ext} is the integral of the sum of the products of shear traction and displacement, σ_s and u_s, and normal traction and displacement, σ_n and u_n, along the boundaries of the model, B:

$$W_{ext}=\oint\!\!\!\oint_B(\sigma_s u_s+\sigma_n u_n)dB \quad (1)$$

W_{ext} reflects the overall mechanical efficiency of a system, such that the most efficient fault propagation path will produce the maximum change in external work, ΔW_{ext}, which is calculated as the difference in W_{ext} before and after fault propagation. Unlike alternative methods of modeling fault growth, work minimization provides a global approach that considers the energy expended in deformational processes throughout the system. Searching for the most efficient system with work minimization is an optimization problem, and so work *minimization* and work *optimization* may be used interchangeably.

In the following sections, we describe the GROW algorithm and the functionality of Fric2D (Cooke and Pollard, 1997), which GROW repeatedly executes to calculate W_{ext} and thereby model fracture growth. Madden et al. (submitted for publication) verify the GROW algorithm by comparing GROW propagation paths to other predictions of fault growth, and validates this tool by comparing GROW results to laboratory observations. In this paper, we show an application of GROW to two crustal-scale strike-slip faults separated by a releasing step, because a significant advantage of GROW is its application to the mixed-mode propagation of faults, which occurs as the faults interact. We analyze the numerical error of these models produced by discretization. We show that the evolution of W_{ext} closely parallels the propagation paths of the modeled faults, and that changes in W_{ext} can indicate when the modeled faults transfer stress through soft- and hard-linkage.

2. Algorithm

The validated numerical modeling tool GROW, which is available under a free and open source license, models the evolution of a fracture network by iteratively searching for the geometry of fracture growth that maximizes the change in external work due to that growth, ΔW_{ext}, divided by fracture area propagated in each increment of growth, ΔA. We use $\Delta W_{ext}/\Delta A$ because systems with more fracture area are more efficient than systems with less fracture area due to the fact that they can accommodate more strain under the same loading. GROW calculates fracture area by considering fractures to have one unit width because it is a two-dimensional, plane strain modeling tool.

To model fracture propagation, GROW first calculates the initial external work of the system, W_{ext}. Next, GROW identifies the most efficient fracture geometry by (1) deforming the system and calculating $\Delta W_{ext}/\Delta A$ for the first fracture geometry, (2) modifying the geometry in the input file to calculate $\Delta W_{ext}/\Delta A$ for each additional radial potential growth orientation, and (3) identifying the geometry that maximizes $\Delta W_{ext}/\Delta A$. After GROW finds the most efficient geometry, this geometry is set as the new fracture geometry to which GROW now adds potential growth elements. GROW will continue to simulate fracture propagation by repeating the steps above until all of the fractures in the system intersect other fractures or the boundary of the model, or if none of the tips of the fractures fail in tension or shear.

In each propagation step, the most efficient fracture geometry maximizes the magnitude of $\Delta W_{ext}/\Delta A$. However, the boundary conditions of the system will determine whether W_{ext} increases or decreases with fracture growth. When displacements are prescribed to the model boundaries, fracture growth decreases the tractions along the boundaries and W_{ext} decreases (Eq. (1)). If tractions are prescribed to the boundaries, fracture growth increases the displacements of the boundaries and W_{ext} increases. Mixed boundary conditions that include tractions on some model boundaries and displacements on others only provide reliable analysis of W_{ext} if one of these conditions is set to zero. Under these conditions, the model boundaries with either tractions or displacements set to zero do not contribute to W_{ext} (Eq. (1)). For reliable GROW models, all of the non-zero boundary conditions should be either displacement or traction conditions. Either of these loading conditions may be prescribed to analyze the increasing mechanical efficiency of a fracture network with GROW, but displacement boundary conditions typically result in faster execution times and more numerically stable results.

2.1. Fric2D and GROW input

GROW uses the two-dimensional boundary element method numerical modeling tool Fric2D (Cooke and Pollard, 1997) to calculate the stresses and displacements within the deforming fracture system. Fric2D solves the quasi-static equations of deformation on each element to determine the displacement and tractions produced by a given set of boundary conditions and influenced by the fracture geometry. Fractures and boundaries are discretized into linear elements of constant displacement discontinuity. Each linear element defines the edge of a fracture plane that is one unit length (e.g., one meter) in width within the plane strain system. The fractures may open or slip, but may not interpenetrate, in response to tractions or displacements applied to the model boundaries, or from opening or slip along nearby elements.

Following a tension positive sign convention, opening occurs when the normal stress along an element meets or exceeds its tensile strength. Slip occurs when the shear stress meets or exceeds its frictional shear strength, which is the difference between its cohesion and the product of normal stress and the coefficient of friction along the fault. Fric2D uses the penalty method for frictional slip with prescribed shear and normal stiffness along fault elements to ensure that the elements do not interpenetrate (e.g., Cooke and Pollard, 1997; Maerten et al., 2010). Additionally, Fric2D 3.2.7 can simulate slip-weakening behavior along pre-existing fractures and/or potential growth elements (Savage and Cooke, 2010). When an element slips beyond a prescribed slip-weakening distance, the coefficient of friction along that element evolves linearly from its static to its sliding value.

To simulate fracture propagation with GROW, the user defines the boundary conditions and initial fracture geometry in a Fric2D input file. This input file also describes how the initial fractures can grow. The user can specify that propagation will occur from one point, multiple points, at one tip of one fracture, at both tips of one fracture, at multiple tips of multiple fractures or any combination of points and fracture tips. Because Fric2D is a boundary element method modeling tool, fracture propagation in GROW is achieved simply by the addition of a single element to the propagating fracture tip. This direct approach differs from many finite element method simulations of propagation, which require re-meshing or constrain propagation paths to the boundaries of pre-existing elements (e.g., Lisjak and Grasselli, 2014).

2.2. Propagation of one fracture tip

To simulate propagation with GROW, the user must specify three angles that describe the orientations of potential radial growth elements: the minimum and maximum angle to test, θ_{min}, θ_{max} respectively, and the resolution angle, θ_r, which determines the number of radial growth orientations tested in each increment of growth. If the initial input file specifies growth from one tip of one fracture, GROW adds a new element at the tip of that fracture oriented θ_{min} clockwise from the tip of the fracture, and calculates $\Delta W_{ext}/\Delta A$ from the Fric2D output (Fig. 1). Except in cases of intersection (Section 2.6), the added element has the same length as the elements of the initial fracture to ensure the stability of the displacement discontinuity method. Next, GROW adds an element at $\theta_{min}+\theta_r$ to the initial input geometry and calculates $\Delta W_{ext}/\Delta A$ for this new geometry. GROW continues calculating $\Delta W_{ext}/\Delta A$ for systems with different potential growth elements up to, but not including, θ_{max}. At the end of this search, GROW identifies the orientation of the potential element, θ_{opt}, that maximizes $\Delta W_{ext}/\Delta A$ and thus optimizes the work of the system. If an element does not fail in shear or tension, no slip or opening occurs on it and the efficiency of the system does not change, so $\Delta W_{ext}=0$. If $\Delta W_{ext}=0$ for all potential elements, propagation is arrested and the GROW run terminates.

After all potential elements have been evaluated, and if at least one potential growth element has failed, GROW refines the search by finding $\Delta W_{ext}/\Delta A$ of the system with an element oriented at $\theta_{opt}+\theta_r/2$ and the system with an element oriented $\theta_{opt}-\theta_r/2$. This additional step of the algorithm allows GROW to first search a wide range of parameter space and then exact a higher-resolution search close to the most efficient orientation found during the first search. After GROW finds the most efficient growth orientation at this fracture tip, GROW uses this efficient fracture geometry as the initial input file for the next propagation step. In this subsequent step, GROW searches for the most efficient orientation of an element at the tip of the previously added element, which is now the new fracture tip.

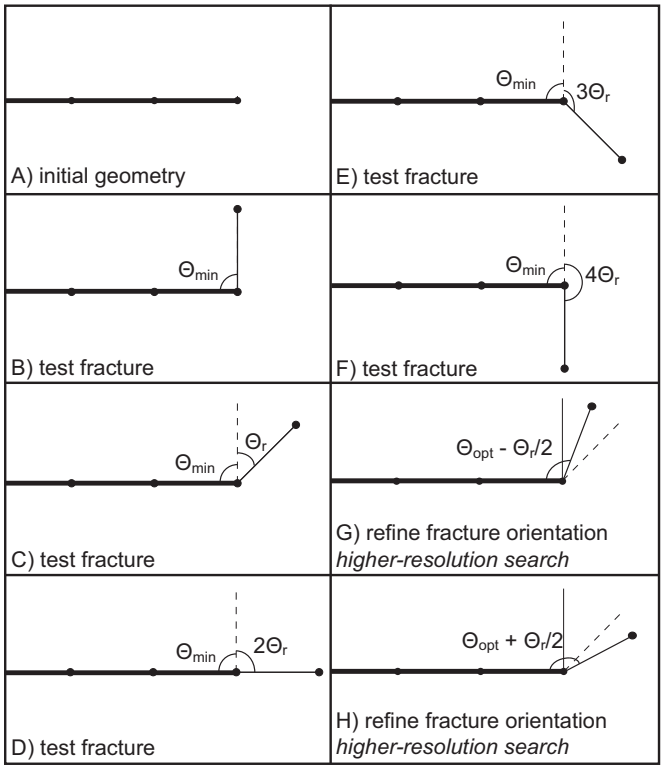

Fig. 1. Potential growth elements tested in an iteration of fracture growth when minimum angle, $\theta_{min}=90°$, resolution angle, $\theta_r=45°$, and maximum angle$=\theta_{min}+C\theta_r$ (where $C>4$ in this example). Thin lines show potential growth elements. Thicker lines show initial geometry. (A) Initial fracture geometry. (B–F) Potential growth elements tested in first, lower-resolution search. Dashed line shows orientation θ_{min} clockwise from tip. (G and H) Geometries tested in higher-resolution search. Orientation of potential element that maximizes $\Delta W_{ext}/\Delta A$ in first broad search of this propagation is $\theta_{min}+\theta_r$. In (G and H) dashed line shows location of most efficiently oriented element identified in first lower resolution search.

2.3. Propagation of multiple fracture tips

When two fracture tips are propagating, GROW searches for and adds the most efficient element oriented from the tip of one fracture, θ_{opt1}, without refining the search for the most efficient element at that fracture tip (Fig. 2a). GROW then uses the new Fric2D input file with the newly added potential element as the starting input file to test the orientation of elements added to the tip of the second fracture (Fig. 2b). After the most efficient orientation is found for the second fracture, θ_{opt2}, GROW refines the search by calculating $\Delta W_{ext}/\Delta A$ for all combinations of $\theta_{opt1}\pm\theta_r/2$ and $\theta_{opt2}\pm\theta_r/2$ shown in Fig. 2d–g. GROW then uses the most efficient geometry identified after this refined search as the input

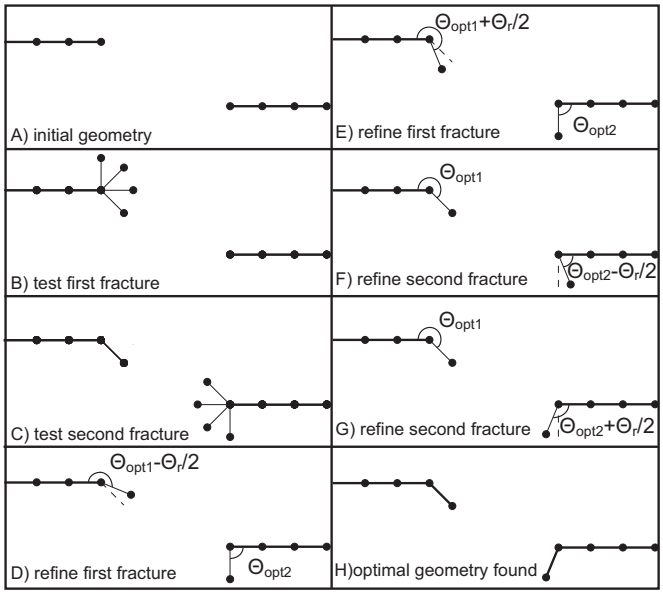

Fig. 2. Illustration of GROW algorithm when two fractures are propagating. Thin lines show potential growth elements. Thicker lines show most efficient geometry identified by GROW. (A) Initial fracture geometry. (B) Potential growth elements tested in first iteration of propagation for upper fracture. (C) Potential growth elements tested in first iteration of growth for lower fracture. (D–G) Geometries tested in higher-resolution search. Dashed lines show elements that optimized work for upper and lower fracture in first lower resolution search (B and C). (H) Most efficient geometry identified in this iteration.

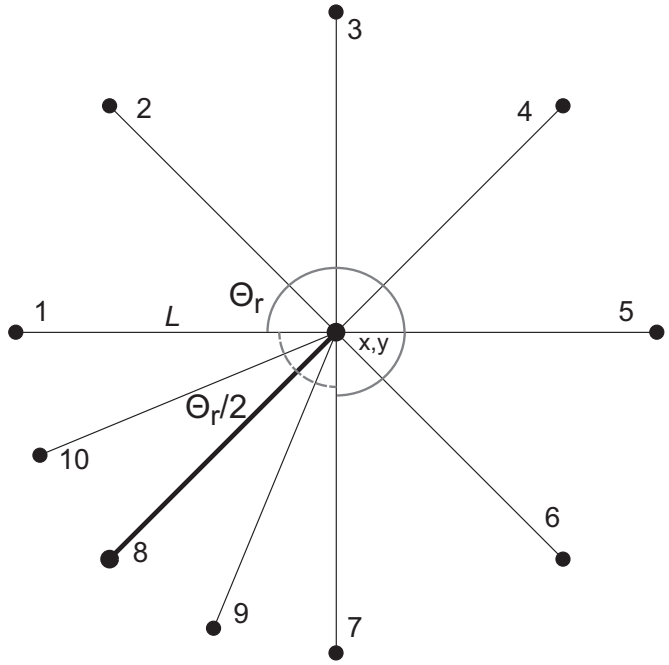

Fig. 3. Example of fracture geometries tested in an iteration of growth when user investigates fracture initiation at a point with resolution angle, θ_r,=45°. Numbers indicate order of orientations along which GROW adds elements and calculates $\Delta W_{ext}/\Delta A$. User prescribes position (*x*,*y*) and length of one element, *L*. Element labeled with 8 is most efficiently orientated element identified in first, lower-resolution search, and elements 9 and 10 are potential growth elements tested within fine-tuning step.

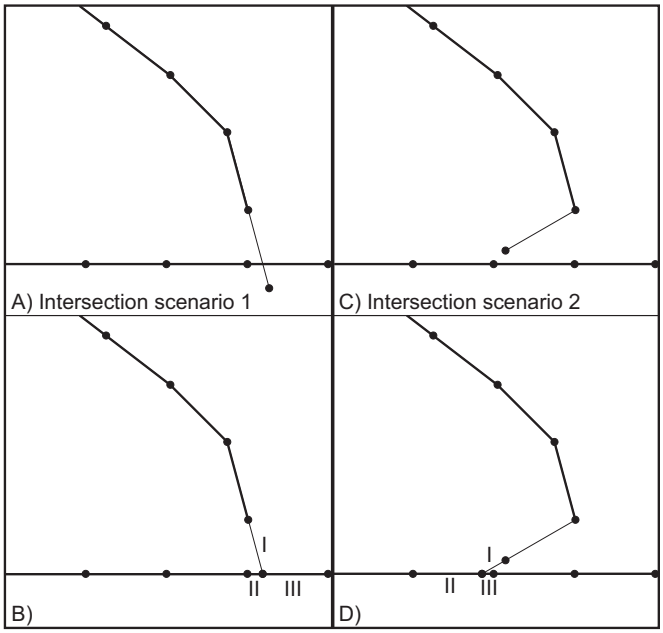

Fig. 4. Detection of fracture intersection and subsequent modification of element nodes. (A) In intersection scenario one, a potential growth element intersects a pre-existing fracture. To maintain kinematic compatibility among elements, GROW replaces propagation element tip with smaller element I, and divides an element of lower fracture into two smaller elements (labeled II and III) (B). (C) In intersection scenario two, GROW detects fracture intersection because tip of newly added element (thin line) falls within one element half-length of lower fracture. As a result, GROW adds a smaller element (labeled I) to tip of upper, propagating fracture, and divides element of lower fracture into two elements labeled II and III (D).

file for the next propagation step. Additionally, GROW can investigate the initiation of fracture by searching for the optimal orientation of a fracture at one or more prescribed points (Fig. 3, and Supplementary material).

2.4. Evolving fracture properties

To simulate the process of failure at the tip of a fracture propagating through intact rock, the properties of the fracture elements evolve as their status changes from potential growth elements to fracture elements. Potential growth elements, which may or may not become fracture elements, should have properties consistent with those for intact rock (e.g., coefficient of internal friction, inherent shear strength and tensile strength). This set of properties ensures that tensile and/or shear failure of intact rock are assessed for each potential radial path of propagation. After the most efficient potential element is identified and added to the tip of the fracture, GROW assigns to this element the strength properties of the pre-existing fracture (e.g., coefficient of static friction, cohesion) prior to the next increment of growth. This approximates the reduction in strength as a fracture propagates through intact material.

2.5. Termination

A GROW simulation ends when all of the fractures in the system stop propagating. A fracture stops propagating when it intersects a model boundary, intersects itself or another fracture, or if none of the potential growth elements fail in tension or shear. Fig. 4 shows two possible intersection geometries. The first scenario (Fig. 4a and b) occurs when the new element strictly intersects a different fracture or boundary. In this situation, the new element is shortened (Fig. 4b, element I), and a node is added to the element of the other fracture or boundary, and thereby divides the pre-existing element into two elements (Fig. 4b, element II and III) so that the potential fracture tip intersects the other structure at one node. The second scenario (Fig. 4c and d) shows that an element is considered to intersect another element if its tip is within half of the element length of another element. GROW uses this criterion because the stresses within this distance of displacement discontinuity elements can be unrealistically high, which will generate an unrealistic assessment of failure. When a potential growth element falls within this distance, GROW adds an additional node to the nearby boundary or fracture element, which produces two new elements (Fig. 4d, element II and III), and adds a smaller element to the tip of the potential fracture element (Fig. 4d, element I), so that the elements link at one node. GROW identifies the most efficient growth orientation with $\Delta W_{ext}/\Delta A$ so that longer elements, which may have more slip, are not favored over shorter elements, when intersection geometries require varying element length.

Additionally, a fault will stop propagating in GROW if none of the potential growth elements fail in either tension or shear. An element fails in tension when the normal stress across its surface, σ_n, which is positive when tensile, exceeds or equals the tensile strength of the intact material at the fault tip, T_o:

$$\sigma_n \geq T_o \tag{2}$$

A potential growth element fails in shear following the Coulomb criterion, when the magnitude of the shear stress across its surface, τ, exceeds or equals the difference between the inherent shear strength, S_o, and the product of the internal coefficient of friction, μ_o, and normal stress, σ_n (tension positive), across the potential element:

$$|\tau| \geq S_o - \mu_o \sigma_n \tag{3}$$

By determining if potential elements fail in the given stress conditions, GROW incorporates robust failure criteria that have

been validated by experimental studies (e.g., Sibson, 1977; Zhao, 2000) and field observations (e.g., Anderson, 1951; Nur et al., 1986; Crider and Pollard, 1998). Each potential growth element must fail by one of the above criteria to be considered a possible growth direction, but the propagation direction is selected through work optimization. If an element does not fail in either tension or shear, then W_{ext} equals that of the previous model and $\Delta W_{ext}/\Delta A$ is zero because no slip and/or opening along any new potential element increased the efficiency of the system.

Under certain conditions, modeled faults will continue to propagate for many propagation steps. To free memory and reduce processing time, GROW restarts automatically every five propagation steps. When restarting a subsequent GROW run, GROW uses the identical angle range and resolution (θ_{min}, θ_{max}, θ_r) originally specified by the user, but sets the most efficient geometry found in the previous propagation step as the initial input file.

2.6. Alternative algorithms for the development of multiple fractures

The algorithm implemented in this version of GROW assesses the propagation of multiple fractures sequentially, which provides a balance between computational efficiency and physical robustness. When f tips of fractures are propagating, and a orientations are tested in each increment of growth, GROW executes more than fa Fric2D models. This sequential implementation finds the most efficient radial element from the tip of one fracture before searching for the efficient element at the tip of the other fracture. One preliminary version of GROW propagated fractures simultaneously, rather than sequentially, so that GROW determined the efficiency of systems with all the unique combinations of orientations of fracture tips. However, this algorithm required f^a calculations in each increment of growth. For example, in a simultaneous propagation model with two fracture tips, growth angles from $\theta_{min}=120°$ to $\theta_{max}=240°$, and a resolution angle of 10°, Fric2D must solve the displacement discontinuity equations 4000+ times for each increment of fracture growth. In the current sequential propagation implementation, these input parameters only require ~24 calculations for each growth increment. Future versions of GROW may include a more computationally efficient global optimization algorithm to determine the fracture geometry, such as simulated annealing (e.g., Floudas and Gounaris, 2008), which may permit simultaneous fracture growth.

In most fracture systems, the order in which GROW propagates fractures only influences the resulting geometry when the tips of the fractures closely approach other fractures or boundaries. This influence may vary with loading conditions and fracture geometry. The user may investigate this influence by changing the naming of the fractures, as GROW propagates fractures in alphanumeric order.

3. Application to fault growth

Although GROW can assess both joint and fault propagation, its utility is greatest for fault propagation, because work optimization can directly compare the competing efficiency and likelihood of tensile and shear failure (Cooke and Madden, 2014; Madden et al., Submitted for publication). To demonstrate an application of GROW, we model the propagation and interaction of two kilometer-scale faults separated by a releasing step. We investigate the propagation paths of both faults and report on the evolution of W_{ext} and ΔW_{ext} as the faults grow. We also investigate the effect of element size on the propagation path of the faults and the numerical error caused by discretization.

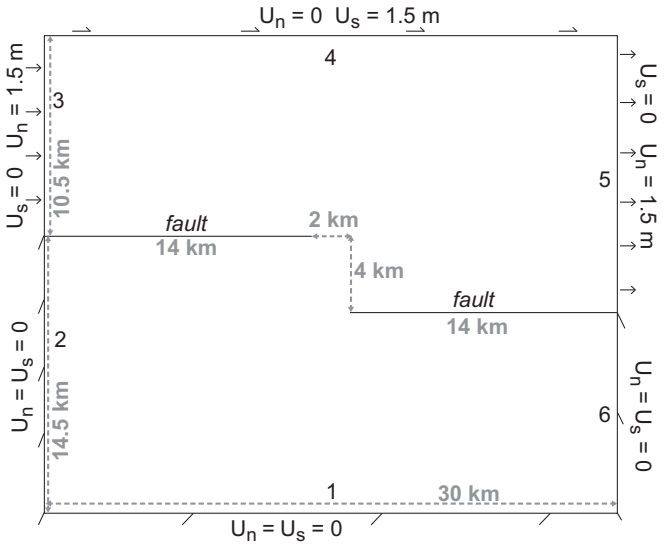

Fig. 5. Boundary conditions and initial geometry of model of releasing step with 4 km of perpendicular separation and 2 km of underlap between faults. Boundaries #1, 2 and 6 have no applied shear (U_s) or normal displacement (U_n), so these boundaries remain fixed as upper part of model moves. $U_n=1.5$ m inward on boundary #3 and $U_n=1.5$ m outward on boundary #5. $U_s=1.5$ m to right on boundary #4 to model a releasing step.

3.1. Input

To model fault growth within a releasing step, we apply displacements along the model boundaries. Fig. 5 shows the boundary conditions and initial fault geometry of 2 km of underlap and 4 km of perpendicular separation between the faults. Boundaries #1, 2 and 6 remain stationary as the upper portion of the model moves. We prescribe rightward normal displacement of 1.5 m on boundaries #3 and #5, inward and outward respectively. We set 1.5 m of rightward shear displacement along boundary #4, which is consistent with the prescribed normal displacement along the upper side boundaries (#3 and 5). Table 1 presents the intact rock and fault characteristics used in this model. We use intact rock and fault properties similar to values estimated for granite (e.g., Hoek and Brown, 1997). However, in this example we promote shear failure by using an elevated tensile strength for intact granite of $T_o=18$ MPa, which is somewhat larger than the estimated average T_o of ~0.01–1 MPa (Hoek and Brown, 1997). Lower values of T_o would favor wing-crack propagation as opposed to shear failure, which we wish to demonstrate in these models.

We specify the potential element orientation range that GROW

Table 1
Fault and intact rock parameters used in GROW application. Intact rock properties are prescribed to all potential elements that radiate from tip of propagating fault to assess failure potential of each propagation orientation. Fault properties are prescribed to elements of fault geometry that optimize work.

Property		Value
Intact rock	Poisson's ratio	0.17
	Young's modulus	50 GPa
	Tensile strength	18 GPa
	Inherent shear strength	7 MPa
	Internal friction	0.5
Fault	Initial cohesion	0 MPa
	Sliding cohesion	0 MPa
	Static friction	0.3
	Dynamic friction	0.3
	Slip-weakening distance	0 m

searches with a resolution angle of $\theta_r = 15°$, a minimum angle of $\theta_{min} = 150°$, and a maximum angle of $\theta_{max} = 270°$. We execute three GROW models that differ only by the element length of the faults and boundaries, L, which we set as 125 m, 250 m, and 500 m. For propagation to appropriately respond to the concentration of stresses at fracture tips, the length of elements comprising a fracture in a boundary element method model should be less than 1% of the total fracture length (e.g., Madden et al., Submitted for publication). The initial fracture geometry of the models shown here simulate half of two 28 km faults, so elements with length < 280 m will produce greater accuracy. We show results of a model with an element length greater than the recommended size (500 m), and two models with element length within the recommended range to demonstrate the effect of selecting element sizes greater and less than this critical value.

The solutions for inelastic systems, such as those with frictional slip, can vary with number of loading steps (e.g., Cooke and Pollard, 1997). However, if the loading of the system is at or very near failure, such as our application, then increasing the number of loading steps has negligible impact on the solution because the system is elastic until it fails. For the $L = 125$ m model of our application, the ΔW_{ext} due to increasing the number of loading steps by an order of magnitude for the initial model geometry is ~4% of the minimum ΔW_{ext} due to fault propagation calculated for any growth increment in the evolution of the system. Applying the displacement in only one loading increment likely does not strongly influence the efficiency of the orientation determined by GROW for the application presented here.

3.2. Results

For the three models investigated in this GROW application, the faults propagate toward each other and eventually link (Fig. 6, and animations in the Supplementary material). In the models with $L = 125$ m and 250 m, the faults propagate collinearly for ~2.9 km before each begins to propagate toward the opposite fault. In contrast, in the model with $L = 500$ m, the faults propagate out-of-plane, at 187.5° clockwise to the fault tip and toward the opposite fault, in the first iteration of growth. The propagating tips of the faults with $L = 500$ m intersect one another closer to the center of the model than in the models with smaller elements because these faults immediately begin propagating out-of-plane toward the adjacent fault.

To further demonstrate the effect of element size, we show the numerical error produced by discretization for models with $L = 500$ m, 250 m, 125 m, 62.5 m, and 31.25 m (Fig. 7a). Here, we calculate the discretization error of a model with an element size of L as the difference in W_{ext} between a model with element size L and a model with element size $2L$ because the exact analytical solution of W_{ext} for this system is not currently known, and may not exist. For example, the discretization error calculated for the model with $L = 125$ m is the initial W_{ext} of the $L = 125$ m model subtracted by the initial W_{ext} for the $L = 250$ m model. The discretization error decreases with increasing number of elements approximately as a power law with an exponent of -0.97 (Fig. 7a). This asymptotic convergence rate suggests that defining discretization error as the difference in W_{ext} between models with different element sizes provides a viable approximation of the numerical error due to discretization in the absence of an exact analytical solution.

The computational time required to run one Fric2D model of the initial fracture geometry with the five aforementioned element sizes on one CPU of a 64 bit quad-core Linux server increases as element size decreases as a power law with an exponent of ~3.3 (Fig. 7a). The exponents, or rates of convergence, of the best-fit power laws of the run time and discretization error reveal that run time increases much more rapidly than discretization error decreases for this range of element sizes. The total run time for a complete GROW propagation sequence depends on the time required to run one Fric2D model, the number of fracture geometries tested within one increment of growth, and the total number of increments of fracture growth in the GROW run. The number of increments of growth, run time of an individual model with $L = 125$ m, and angle range and resolution of search for the efficient orientation produced a total run time of ~2.5 weeks for this model. Future implementations of GROW will explore parallelizing the search for efficient fracture geometries to take advantage of distributed CPU.

The distribution of ΔW_{ext} for each potential element added to the tip of the lower right fault in the first growth increment indicates that some of the potential elements ($\theta = 150°$, 240°) did not meet either failure criterion implemented in GROW, as $\Delta W_{ext} = 0$

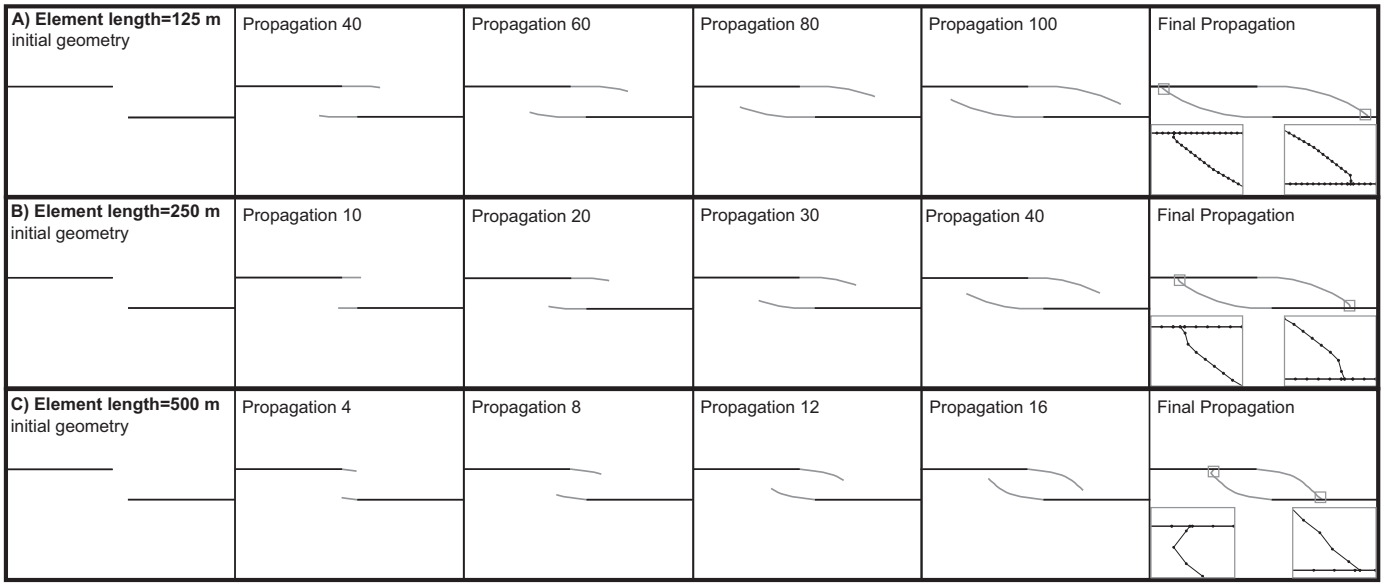

Fig. 6. Propagation path of faults for model with 125 m element length (A), 250 m element length (B), and 500 m element length (C). Initial fault geometry colored in black lines. Faults propagated by GROW colored in gray lines. For all models, faults propagate toward adjacent fault until they link. Inset gray boxes show details of fault intersection and nodes of each element in final propagation step. Each gray box has equal area, so differing element size may be directly compared.

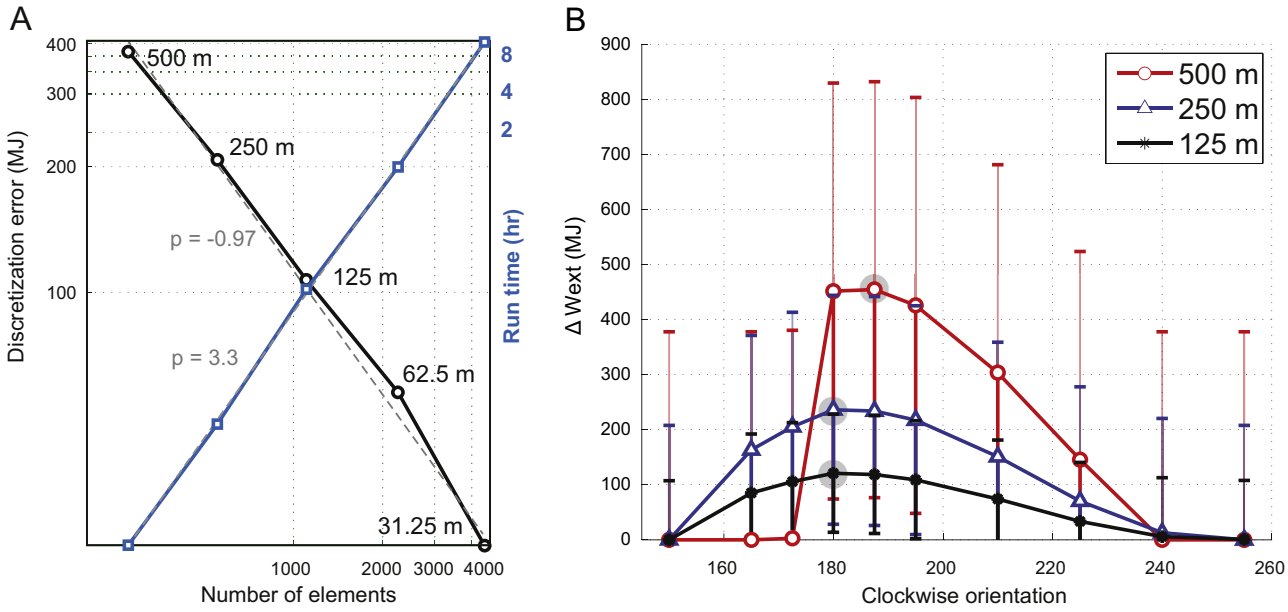

Fig. 7. Discretization error analysis. (A) Numerical error induced by discretization, and run time of models, for element length = 31.25 m, 62.5 m, 125 m, 250 m, and 500 m. Numerical error of model with element length, L, is difference of initial W_{ext} of models of element lengths L and 2 L. With increasing element number, numerical error decreases as a power law with an exponent, p, of ~ -1, while run time increases as a power law with $p = \sim 3$. (B) ΔW_{ext} for each potential growth element added to lower fault in first increment of growth for element length, $L = 125$ m, 250 m, and 500 m. Orientation of element measured clockwise from fault tip. For $L = 125$ m and 250 m, element oriented 180° maximizes ΔW_{ext} and minimizes W_{ext}. For $L = 500$ m, the element oriented at 187.5° maximizes ΔW_{ext}. Gray circle highlights most efficient potential element orientation for each model. Error bars of each model in (B) are equal to discretization error shown in (A).

for these orientations (Fig. 7b). The discretization errors calculated for each model are less than the amplitude of each respective ΔW_{ext} curve, and as the element size decreases, the predicted orientation of the most efficient element converges to the same value (Fig. 7b). These relationships lend support to the supposition that GROW can discern the optimal growth orientations in this system.

The evolution of W_{ext} with fault growth for the model with $L = 125$ m indicates that as the faults propagate under the applied displacements, W_{ext} decreases and the overall mechanical efficiency of the fault system increases (Fig. 8a). In GROW models, the evolution of the system due to fracture growth serves as a proxy for time, so we refer to the change in efficiency rate (ΔW_{ext}) as *propagation power* because power is the rate of change in work with respect to time. The largest increase in propagation power occurs when the faults hard-link to one another in the final propagation step (Fig. 8b). Generally, propagation power decreases as the faults grow until it begins to increase late in the development of this fault system when the faults approach one another (> 25 km*m total new fault area in Fig. 8b). After that point, the propagation power quickly increases with fault growth. This increase in propagation power starts when the tips of the faults are ~ 2 km from each other and begin to propagate more directly toward each other.

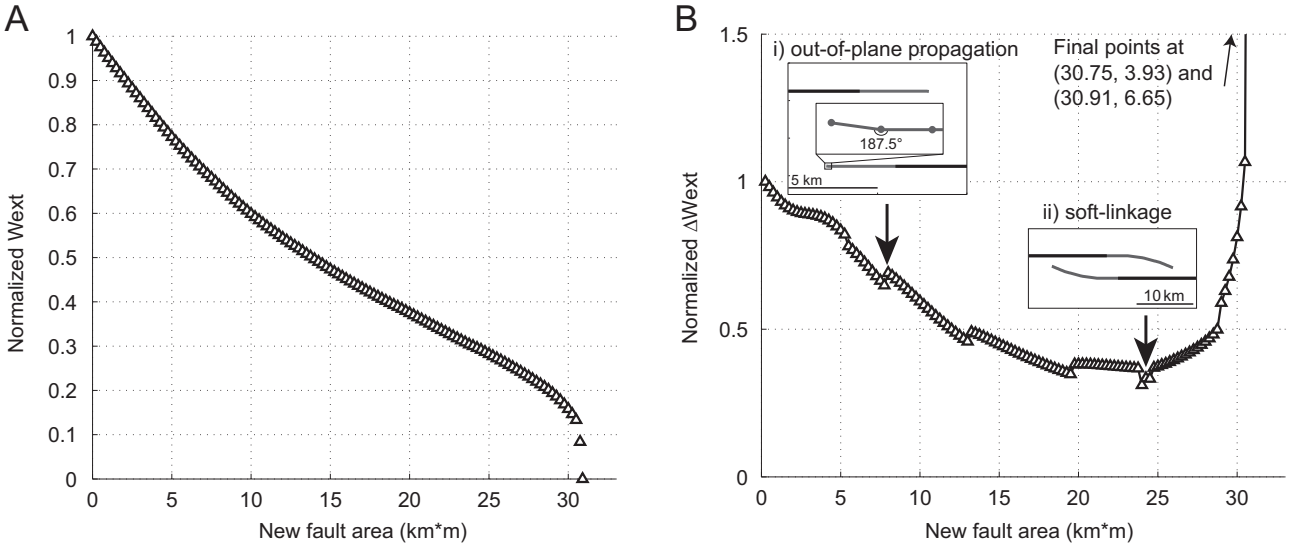

Fig. 8. Evolution of W_{ext} with fault growth for 125 m element length model. (A) Normalized W_{ext} is W_{ext} of each growth increment/initial W_{ext}. With each increment of fault growth, the normalized W_{ext} decreases, and thus efficiency increases. (B) Normalized propagation power is ΔW_{ext}/initial ΔW_{ext}. Propagation power deviates from general decreasing trend and increases when faults deflect toward each other. The largest increase in efficiency occurs when faults hard-link. (Bi) Fault geometry that produces increase in ΔW_{ext} due to out-of-plane propagation toward other fault. (Bii) Fault geometry associated with soft-linkage, when propagation power begins to continually increase as tips of faults closely approach adjacent fault before hard-linkage.

Before ~25 km*m new fault area has propagated, episodic increases in propagation power are followed by periods of decreasing propagation power. These transient increases in propagation power occur when the faults do not propagate exactly inline ($\theta \neq 180°$). The non-collinear propagation at one fault tip, at 187.5° clockwise from the tip, produces this first transient increase in propagation power (Fig. 8b, inset i). Similar episodic increases in propagation power occur at two additional instances in the evolution of the fault network, and similarly correspond to when the faults propagate out-of-plane.

3.3. Discussion

This application of GROW demonstrates that the evolution of propagation power is closely related to the propagation path of the modeled faults. When the faults first begin to propagate, the system becomes increasingly efficient with relatively high propagation power. Propagation power then decreases as each increment of growth contributes a smaller gain in efficiency, except when the fault propagation paths periodically propagate along a more direct path towards the adjacent fault (Fig. 8b, i). The increase in propagation power as the faults grow within 2 km of each other, and their propagation paths deflect towards each other, shows that work minimization can detect the interaction between, and soft-linkage of the faults. The most significant increase in propagation power occurs when the faults hard-link through the releasing step in the final propagation increment (Fig. 6a). This hard-linkage causes W_{ext} to decrease to ~0 J/m^2 in the final increment (Fig. 8a) because the faults intersect each other.

Previous workers have identified soft-linkage from the slip distribution of faults. In contrast to isolated fault segments that host an elliptical slip distribution along strike according to classical linear elastic fracture mechanics (e.g., Pollard and Segall, 1987), or a bell-shaped distribution following elastic–plastic theory (e.g., Cowie and Scholz, 1992), fault segments that interact, but have not hard-linked, often display an asymmetric slip distribution profile with maximum slip shifted toward the nearby fault (e.g., Manighetti et al., 2001; and references therein). If the aggregate slip distribution of all the faults in a network produces an approximately elliptical shape, then individual fault segments within the network are considered to function as one coherent structure (e.g., Soliva and Benedicto, 2004; and references therein) and may be identified as soft-linked. Individual faults will function as one structure when the stress perturbations produced by slip on or propagation of a fault in the network affects any nearby faults. In the application of GROW shown here, we identify soft-linkage as when fault interaction begins to contribute to relatively large gains in efficiency (Fig. 8b, ii), but before the faults link to each other.

Slip profiles of the modeled fault network at two stages of growth, which encompass the increment when we identify soft-linkage through ΔW_{ext}, show that as the faults propagate, slip along the parallel traces of the faults decrease, while additional slip is accommodated near the growing fault tips (Fig. 9). The soft-linkage of the faults, after GROW has propagated 24 km*m of new fault area, promotes slip transfer between the faults and increases slip near the tips of the faults. The increasing efficiency of the system shown by ΔW_{ext}, and the change in the slip distribution suggest the transfer of stress through soft-linkage.

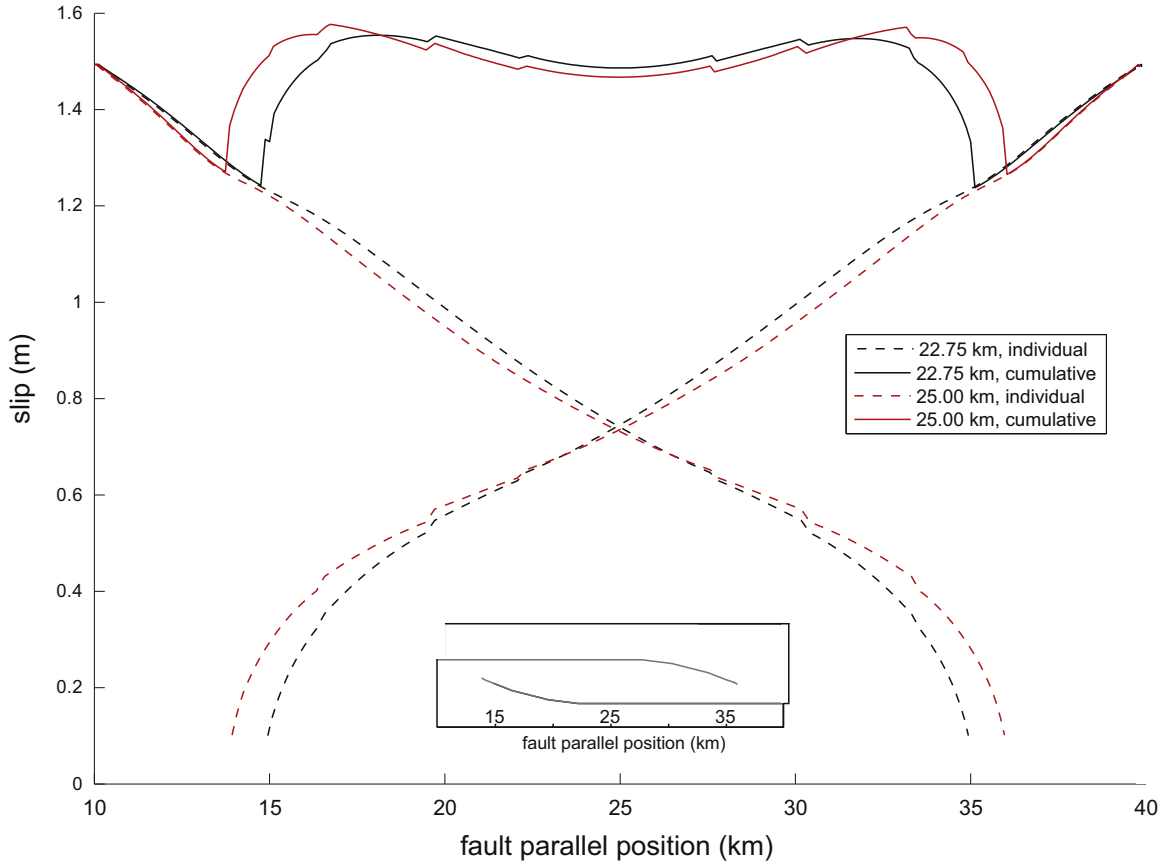

Fig. 9. Individual (dashed lines) and cumulative slip profiles of faults at two stages of growth near when ΔW_{ext} suggests soft-linkage for $L = 125$ m. Black lines show slip profile when new fault length added is 22.75 km, and red lines show profile when new fault length added is 25 km. ΔW_{ext} suggests soft-linkage when new fault length added is 24 km (Fig. 8b). Soft-linkage of faults increases slip near fault tips. Inset shows fracture geometry when new fault added is 25 km. (For interpretation of the color references, please see the web version of this article.)

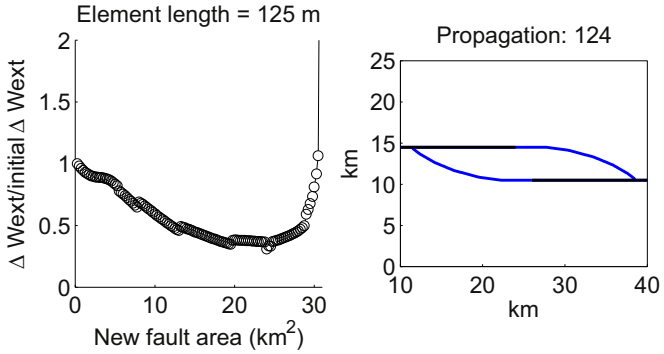

Video 1. Evolution of normalized ΔW_{ext} (left) and fault geometry (right) for model with element length, $L=125$ m. Normalized $\Delta W_{ext}=\Delta W_{ext}$ divided by ΔW_{ext} of first increment of growth. Propagation number on right indicates the number of growth increments elapsed. Black lines indicate initial fault geometry. Blue lines indicate newly propagated fault. A video clip is available online. Supplementary material related to this article can be found online at http://dx.doi.org/10.1016/j.cageo.2015.12.019.

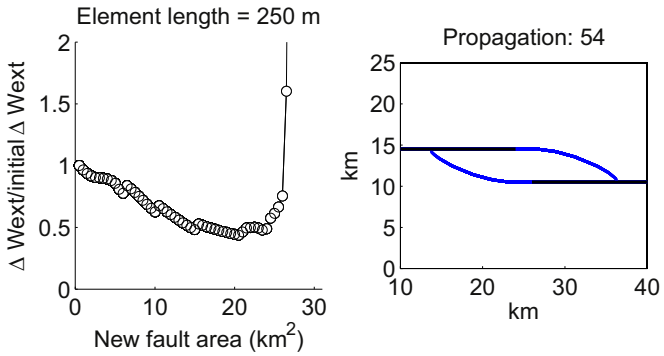

Video 2. Evolution of normalized ΔW_{ext} (left) and fault geometry (right) for model with element length, $L=250$ m. Normalized $\Delta W_{ext}=\Delta W_{ext}$ divided by ΔW_{ext} of first increment of growth. Propagation number on right indicates the number of growth increments elapsed. Black lines indicate initial fault geometry. Blue lines indicate newly propagated fault. A video clip is available online. Supplementary material related to this article can be found online at http://dx.doi.org/10.1016/j.cageo.2015.12.019.

For all three models, the first-order similarities of the final fault geometries are striking considering that the element size differs by a factor of four, which corresponds to a difference of more than 800 elements. The variation of the $L=500$ m model from the $L=125$ m and 250 m models may reflect inaccuracy arising from the inability of the long element ($>$ 1% total fracture length) to respond to the localized fracture tip stress field. In each model, the faults in the releasing step propagate toward the adjacent fault and eventually link with the opposite fault. These modeled paths resemble the pattern of faulting often observed in natural releasing steps (e.g., Cunningham and Mann, 2007).

The discretization errors calculated for each model are less than the amplitude of each respective ΔW_{ext} curve, and as the element size of the models decrease, the optimal orientation predicted by GROW converges to the same value (Fig. 7b). These relationships lend confidence to the propagation paths predicted by GROW, because they imply that the most mechanically efficient orientation of potential fault growth element can be differentiated from less optimally oriented elements within the error margin.

4. Conclusions

GROW can predict fracture initiation, non-linear propagation, and interaction between multiple fractures through intact rock by iteratively searching for the radial propagation path that optimizes the external work of the system, and thus its overall efficiency. The work optimization approach implemented in GROW provides the functionality to model the evolution of fracture networks in a broad range of tectonic environments that follow complex propagation paths. Similar to the maximum Coulomb stress and energy release rate criteria, GROW can be used to investigate the mode-I failure and propagation of joints and veins. GROW also can predict the complex, out-of-plane propagation paths of faults and fractures that propagate by both shear and tensile failure. This work optimization approach directly compares the efficiency of shear and tensile failure at a fracture tip and so predicts a unique propagation path at every increment of growth. Additionally, this boundary element method approach allows fracture propagation to be modeled simply by adding an element to a fracture tip, and does not require complex re-meshing. GROW allows the user to set the intact rock properties, fracture properties, initial fracture geometry, and boundary conditions in order to simulate a specific system or test a general hypothesis. The application of GROW shown here demonstrates that element size can influence the final fault geometry, but that the first-order shape of the final fault geometry remains relatively similar even when element size differs by a factor of four. The evolution of propagation power, as calculated from GROW output, provides significant information about fault interaction and delineates the timing of soft- and hard-linkage.

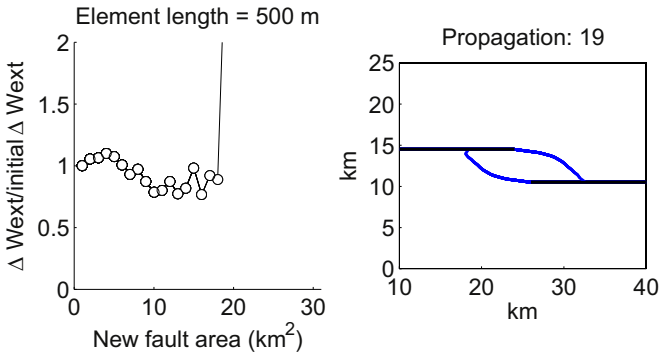

Video 3. Evolution of normalized ΔW_{ext} (left) and fault geometry (right) for model with element length, $L=500$ m. Normalized $\Delta W_{ext}=\Delta W_{ext}$ divided by ΔW_{ext} of first increment of growth. Propagation number on right indicates the number of growth increments elapsed. Black lines indicate initial fault geometry. Blue lines indicate newly propagated fault. A video clip is available online. Supplementary material related to this article can be found online at http://dx.doi.org/10.1016/j.cageo.2015.12.019.

Acknowledgments

This work was supported by NSF Grant EAR-1219919. We thank Aviel Stern for detailed critiques of the GROW User Manual and three anonymous reviewers for helpful comments and suggestions that improved the manuscript.

Appendix A. Supplementary material

Supplementary data associated with this article can be found in the online version at http://dx.doi.org/10.1016/j.cageo.2015.12.019.

References

Anderson, C.M., 1951. The Dynamics of Faulting. Oliver and Boyd, Edinburgh.
Cooke, M.L., Kameda, A., 2002. Mechanical fault interaction within the los angeles basin: a two-dimensional analysis using mechanical efficiency. J. Geophys. Res.

107, 1–15.
Cooke, M.L., Madden, E.H., 2014. Is the Earth lazy? A review of work minimization in fault evolution. J. Struct. Geol. 66, 334–346. http://dx.doi.org/10.1016/j.jsg.2014.05.004.
Cooke, M.L., Pollard, D.D., 1997. Bedding plane slip in initial stages of fault-related folding. J. Struct. Geol. 19, 567–581.
Cowie, P.A., Scholz, C.H., 1992. Physical explanation for the displacement-length relationship of faults using a post-yield fracture mechanics model. J. Struct. Geol. 14, 1133–1148.
Crider, J.G., Peacock, D.C.P., 2004. Initiation of brittle faults in the upper crust: a review of field observations. J. Struct. Geol. 26, 691–707. http://dx.doi.org/10.1016/j.jsg.2003.07.007.
Crider, J.G., Pollard, D.D., 1998. Fault linkage: three-dimensional mechanical interaction between echelon normal faults. J. Geophys. Res. 103 (B10), 24373 ⟨http://doi.org/10.1029/98JB01353⟩.
Cubas, N., Leroy, Y.M., Maillot, B., 2008. Prediction of thrusting sequences in accretionary wedges. J. Geophys. Res.: Solid Earth 113, B12412. http://dx.doi.org/10.1029/2008JB005717.
Cunningham, W.D., Mann, P., 2007. Tectonics of strike-slip restraining and releasing bends. Geol. Soc. Lond. Spec. Publ. 290, 1–12.
Del Castello, M., Cooke, M.L., 2007. Underthrusting-accretion cycle: work budget as revealed by the boundary element method. J. Geophys. Res. 112, 1–14.
De Bremaecker, J., Ferris, M.C., 2004. Numerical models of shear fracture propagation. Eng. Fract. Mech. 71 (15), 2161–2178. http://dx.doi.org/10.1016/j.engfracmech.2003.12.006.
Drucker, D.C., Prager, W., 1952. Soil mechanics and plastic analysis or limit design. Q. Appl. Math. 10, 157–165.
Floudas, C.A., Gounaris, C.E., 2008. A review of recent advances in global optimization. J. Glob. Optim. 45 (1), 3–38. http://dx.doi.org/10.1007/s10898-008-9332-8.
Griffith, A.A., 1924. Theory of rupture. In: Proc. 1st Intern. Congr. Appl. Mech., pp. 55–63.
Gutscher, M.A., Kukowski, N., Malavieille, J., Lallemand, S., 1998. Episodic imbricate thrusting and underthrusting: analog experiments and mechanical analysis applied to the Alaskan Accretionary Wedge. J. Geophys. Res. 103, 10,161–10,176.
Hardy, S., Duncan, D., Masek, J., Brown, D., 1998. Minimum work, fault activity and the growth of critical wedges in fold and thrust belts. Basin Res. 10, 365–373. http://dx.doi.org/10.1046/j.1365-2117.1998.00073.x.
Hoek, E., Brown, E.T., 1980. Underground Excavations in Rock. Inst. Min. Met., London, p. 527.
Hoek, E., Brown, E.T., 1997. Practical estimates of rock mass strength. Int. J. Rock Mech. Min. Sci. 34 (6), 1165–1186.
Irwin, G.R., 1958. Fracture. In: Flugge, S. (Ed.), Encyclopedia of Physics. Springer-Verlag, New York, pp. 551–590.
Jaeger, J.C., Cook, N.G.W., Zimmerman, R.W., 2007. Fundamentals of Rock Mechanics, Fourth Edition Blackwell Publishing, Malden, MA.
Jones, C.H., Wesnousky, S.G., 1992. Variations in strength and slip rate along the San Andreas Fault system. Science 256, 83–86.
Lajtai E. Z., Experimental evaluation of the Griffith theory of brittle failure, Tectonophysics 11, 1971, 129–156.
Lisjak, A., Grasselli, G., 2014. A review of discrete modeling techniques for fracturing processes in discontinuous rock masses. J. Rock Mech. Geotech. Eng. 6, 301–314. http://dx.doi.org/10.1016/j.jrmge.2013.12.007.
Madden, E.H., Cooke, M.L., McBeck, J.A., 2015. Fault propagation and estimates of fault energy budgets using the fault growth modeling tool GRowth by Optimization of Work (GROW). Int. J. Rock. Mech. Min. Sci. (Submitted for publication)
Maerten, L., Gillespie, P., Pollard, D.D., 2002. Effects of local stress perturbation on secondary fault development. J. Struct. Geol. 24 (1), 145–153. http://dx.doi.org/10.1016/S0191-8141(01)00054-2.
Maerten, F., Maerten, L., Cooke, M., 2010. Solving 3D boundary element problems using constrained iterative approach. Comput. Geosci. 14, 551–564. http://dx.doi.org/10.1007/s10596-009-9170-x.
Maillot, B., Leroy, Y.M., 2006. Kink-fold onset and development based on the maximum strength theorem. J. Mech. Phys. Solids 54 (10), 2030–2059. http://dx.doi.org/10.1016/j.jmps.2006.04.004.
Manighetti, I., King, G.C.P., Gaudemer, Y., Scholz, C., Doubre, C., 2001. Slip accumulation and lateral propagation of active normal faults in Afar. J. Geophys. Res. 106 (B7), 13667–13696.
McClintock, F.A., Walsh, J.B., 1962. Friction on Griffith cracks in rocks under pressure. In: Proceedings of the 4th Natl. Congr. Appl. Mech., pp. 1015–1021.
Mogi, K., 1971. Fracture and flow of rocks under high triaxial compression. J. Geophys. Res. 76, 1255–1269.
Nur, A., Ron, H., Scotti, O., 1986. Fault mechanics and the kinematics of block rotations. Geology 14 (9), 746–749. http://dx.doi.org/10.1130/00917613(1986)14<746:FMATKO>2.0.CO;2.
Olson, E.L., Cooke, M.L., 2005. Application of three fault growth criteria to the Puente Hills thrust system, Los Angeles, California, USA. J. Struct. Geol. 27 (10), 1765–1777. http://dx.doi.org/10.1016/j.jsg.2005.02.005.
Olson, J.E., Pollard, D.D., 1991. The initiation and growth of en echelon veins. J. Stuct. Geol. 13 (5), 595–608.
Pollard, D., Aydin, A., 1988. Progress in understanding jointing. Geol. Soc. Am. Bull. 100, 1181–1204.
Pollard, D., Fletcher, R.C., 2005. Fundamentals of Structural Geology. Cambridge University Press, Cambridge.
Pollard, D.D., Segall, P., 1987. Theoretical displacements and stresses near fractures in rock: with applications to faults, joints, veins, dikes, and solution surfaces. In: Atkinson, B.K. (Ed.), Fracture Mechanics of Rocks. Academic Press, London.
Savage, H.M., Cooke, M.L., 2010. Unlocking the effects of friction on fault damage zones. J. Struct. Geol. 32 (11), 1732–1741. http://dx.doi.org/10.1016/j.jsg.2009.08.014.
Savalli, L., Engelder, T., 2005. Mechanisms controlling rupture shape during subcritical growth of joints in layered rocks. Geol. Soc. Am. Bull. 117 (3–4), 436–449. http://dx.doi.org/10.1130/B25368.1.
Schultz, R.A., 1999. Understanding the process of faulting: selected challenges and opportunities at the edge of the 21st century. J. Struct. Geol. 21, 985–993.
Sibson, R.H., 1977. Fault rocks and fault mechanisms. J. Geol. Soc. 133 (3), 191–213. http://dx.doi.org/10.1144/gsjgs.133.3.0191.
Soliva, R., Benedicto, A., 2004. A linkage criterion for segmented normal faults. J. Struct. Geol. 26, 2251–2267.
Souloumiac, P., Leroy, Y.M., Maillot, B., Krabbenhøft, K., 2009. Predicting stress distributions in fold-and-thrust belts and accretionary wedges by optimization. J. Geophys. Res. 114, B09404. http://dx.doi.org/10.1029/2008JB005986.
Souloumiac, P., Krabbenhøft, K., Leroy, Y., Maillot, B., 2010. Failure in accretionary wedges with the maximum strength theorem: numerical algorithm and 2D validation. Comput. Geosci. 14, 793–811. http://dx.doi.org/10.1007/s10596-010-9184-4.
Yagupsky, D.L., Brooks, B.A., Whipple, K.X., Duncan, C.C., Bevis, M., 2014. Distribution of active faulting along orogenic wedges: minimum-work models and natural analogue. J. Struct. Geol. 66, 237–247. http://dx.doi.org/10.1016/j.jsg.2014.05.025.
Zhao, J., 2000. Applicability of Mohr–Coulomb and Hoek–Brown strength criteria to the dynamic strength of brittle rock. Int. J. Rock. Mech. Min. Sci. 37 (7), 1115–1121. http://dx.doi.org/10.1016/S1365-1609(00)00049-6.